

We are IntechOpen, the world's leading publisher of Open Access books Built by scientists, for scientists

6,900

Open access books available

186,000

International authors and editors

200M

Downloads

Our authors are among the

154

Countries delivered to

TOP 1%

most cited scientists

12.2%

Contributors from top 500 universities



WEB OF SCIENCE™

Selection of our books indexed in the Book Citation Index
in Web of Science™ Core Collection (BKCI)

Interested in publishing with us?
Contact book.department@intechopen.com

Numbers displayed above are based on latest data collected.
For more information visit www.intechopen.com



Developments in Electrochemistry: The Phase-Shift Method and Correlation Constants for Determining the Electrochemical Adsorption Isotherms at Noble and Highly Corrosion-Resistant Metal/Solution Interfaces

Jinyoung Chun and Jang H. Chun

Additional information is available at the end of the chapter

<http://dx.doi.org/10.5772/52494>

1. Introduction

To obtain an environmentally clean energy source, many experimental methods have been developed and used to study the adsorption of hydrogen for the cathodic H_2 evolution reaction (HER) and hydroxide for the anodic O_2 evolution reaction (OER) at noble and highly corrosion-resistant metal and alloy/aqueous solution interfaces [1–7]. The cathodic HER is one of the most extensively studied topics in electrochemistry, electrode kinetics, renewable and sustainable energy, etc. It is well known that underpotentially deposited hydrogen (UPD H) and overpotentially deposited hydrogen (OPD H) occupy different surface adsorption sites and act as two distinguishable electroadsorbed H species, and that only OPD H can contribute to the cathodic HER [2–7]. Similarly, one can interpret that underpotentially deposited deuterium (UPD D) and overpotentially deposited deuterium (OPD D) occupy different surface adsorption sites and act as two distinguishable electroadsorbed D species, and that only OPD D can contribute to the cathodic D_2 evolution reaction (DER). However, there is not much reliable electrode kinetic data for OPD H and OPD D, i.e. the fractional surface coverage, interaction parameter, and equilibrium constant for the Frumkin adsorption isotherm, at the interfaces. Also, a quantitative relationship between the Temkin and Frumkin or Langmuir adsorption isotherms has not been developed to study the cathodic HER and DER. Thus, there is a technological need for a useful, effective, and reliable method to determine the Frumkin, Langmuir, and Temkin adsorption isotherms of OPD H and OPD D and related electrode kinetic and thermodynamic parameters. In the following discussions, H and D mean OPD H and OPD D, respectively.

Although the electrochemical Frumkin and Langmuir adsorption isotherms may be regarded as classical models and theories, it is preferable to consider the Frumkin and Langmuir adsorption isotherms for H and D rather than electrode kinetics and thermodynamics equations for H and D because these adsorption isotherms are associated more directly with the atomic mechanisms of H and D [8]. However, there is not much reliable information on the Frumkin and Langmuir adsorption isotherms of H for the cathodic HER and related electrode kinetic and thermodynamic data [1–7]. Furthermore, there is not much reliable information on the Frumkin and Langmuir adsorption isotherms of D for the cathodic DER and related electrode kinetic and thermodynamic data. Because, to the authors' knowledge, the interaction parameter and equilibrium constant for the Frumkin adsorption isotherm of H and D cannot be experimentally and readily determined using other conventional methods [3,7].

To determine the Frumkin, Langmuir, and Temkin adsorption isotherms, the phase-shift method and correlation constants have been originally developed on the basis of relevant experimental results and data. The phase-shift method is a unique electrochemical impedance spectroscopy technique for studying the linear relationship between the phase shift ($90^\circ \geq -\varphi \geq 0^\circ$) vs. potential (E) behavior for the optimum intermediate frequency (f_o) and the fractional surface coverage ($0 \leq \theta \leq 1$) vs. E behavior of the intermediates (H, D, OH, OD) for the sequential reactions (HER, DER, OER) at noble and highly corrosion-resistant metal and alloy/solution interfaces [9–29]. The θ vs. E behavior is well known as the Frumkin or Langmuir adsorption isotherm.

At first glance, it seems that there is no linear relationship between the $-\varphi$ vs. E behavior for f_o and the θ vs. E behavior at the interfaces. Thus, the tedious experimental procedures presented there [e.g. 13, 16, 19–21, 27] have been used to verify or confirm the validity and correctness of the phase-shift method. This is discussed in more detail in the section on theoretical and experimental backgrounds of the phase-shift method. However, note that many scientific phenomena have been interpreted by their behavior rather than by their nature. For example, the wave–particle duality of light and electrons, i.e. their wave and particle behaviors, is well known in science and has been applied in engineering. To explain the photoelectric effect of light, the behavior of light is interpreted as a particle, i.e. a photon, on the basis of the observed phenomena or the measured experimental data. Note that the nature of light is a wave. Similarly, to explain the tunneling effect of electrons, the behavior of electrons is interpreted as a wave on the basis of the observed phenomena or the measured experimental data. Note that the nature of the electron is a real particle, which has a negative charge and a mass. Notably, these wave and particle behaviors are complementary rather than contradictory to each other.

The comments and replies on the phase-shift method are described elsewhere [30–34]. New ideas or methods must be rigorously tested, especially when they are unique, but only with pure logic and objectivity and through scientific procedures. However, the objections to the phase-shift method do not fulfill these criteria. The objections to the phase-shift method are substantially attributed to a misunderstanding of the phase-shift method itself [27, 28]. Note especially that all of the objections to the phase-shift method can be attributed to confusion regarding the applicability of related impedance equations for intermediate frequencies and

a unique feature of the faradaic resistance for the recombination step [35]. The validity and correctness of the phase-shift method should be discussed on the basis of numerical simulations with a single equation for $-\varphi$ vs. θ as functions of E and frequency (f) or relevant experimental data which are obtained using other conventional methods. The lack of the single equation for $-\varphi$ vs. θ as functions of E and f and use of incorrect values of the electrode kinetic parameters or the equivalent circuit elements for the numerical simulations given in the comments result in the confused conclusions on the phase-shift method.

In practice, the numerical calculation of equivalent circuit impedances of the noble and highly corrosion-resistant metal and alloy/solution interfaces is very difficult or impossible due to the superposition of various effects. However, it is simply determined by frequency analyzers, i.e. tools. Note that the phase-shift method and correlation constants are useful and effective tools for determining the Frumkin, Langmuir, and Temkin adsorption isotherms and related electrode kinetic and thermodynamic parameters.

This work is one of our continuous studies on the phase-shift method and correlation constants for determining the Frumkin, Langmuir, and Temkin adsorption isotherms. In this paper, as a selected example of the phase-shift method and correlation constants for determining the electrochemical adsorption isotherms, we present the Frumkin and Temkin adsorption isotherms of (H + D) for the cathodic (HER + DER) and related electrode kinetic and thermodynamic parameters of a Pt-Ir alloy/0.1 M LiOH (H₂O + D₂O) solution interface. These experimental results are compared with the relevant experimental data of the noble and highly corrosion-resistant metal and alloy/solution interfaces [11, 13, 16, 19–21, 23–29]. The interaction parameters, equilibrium constants, standard Gibbs energies of adsorptions, and rates of change of the standard Gibbs energies with θ for the Frumkin, Langmuir, and Temkin adsorption isotherms of H, D, (H + D), OH, and (OH + OD) are summarized and briefly discussed.

2. Experimental

2.1. Preparations

Taking into account the H⁺ and D⁺ concentrations [27] and the effects of the diffuse-double layer and pH [36], a mixture (1:1 volume ratio) of 0.1 M LiOH (H₂O) and 0.1 M LiOH (D₂O) solutions, i.e. 0.1 M LiOH (H₂O + D₂O) solution, was prepared from LiOH (Alfa Aesar, purity 99.995%) using purified water (H₂O, resistivity > 18 MΩ · cm) obtained from a Millipore system and heavy water (D₂O, Alfa Aesar, purity 99.8%). The p(H + D) of 0.1 M LiOH (H₂O + D₂O) solution was 12.91. This solution was deaerated with 99.999% purified nitrogen gas for 20 min before the experiments.

A standard three-electrode configuration was employed. A saturated calomel electrode (SCE) was used as the standard reference electrode. A platinum-iridium alloy wire (Johnson Matthey, 90:10 Pt/Ir mass ratio, 1.5 mm diameter, estimated surface area ca. 1.06 cm²) was used as the working electrode. A platinum wire (Johnson Matthey, purity 99.95%, 1.5 mm

diameter, estimated surface area ca. 1.88 cm^2) was used as the counter electrode. Both the Pt–Ir alloy working electrode and the Pt counter electrode were prepared by flame cleaning and then quenched and cooled sequentially in Millipore Milli-Q water and air.

2.2. Measurements

A cyclic voltammetry (CV) technique was used to achieve a steady state at the Pt–Ir alloy/0.1 M LiOH ($\text{H}_2\text{O} + \text{D}_2\text{O}$) solution interface. The CV experiments were conducted for 20 cycles at a scan rate of $200 \text{ mV} \cdot \text{s}^{-1}$ and a scan potential of (0 to -1.0) V vs. SCE. After the CV experiments, an electrochemical impedance spectroscopy (EIS) technique was used to study the linear relationship between the $-\varphi$ vs. E behavior of the phase shift ($90^\circ \geq -\varphi \geq 0^\circ$) for the optimum intermediate frequency (f_o) and the θ vs. E behavior of the fractional surface coverage ($0 \leq \theta \leq 1$). The EIS experiments were conducted at scan frequencies (f) of (10^4 to 0.1) Hz using a single sine wave, an alternating current (ac) amplitude of 5 mV, and a direct current (dc) potential of (0 to -1.20) V vs. SCE.

The CV experiments were performed using an EG&G PAR Model 273A potentiostat controlled with the PAR Model 270 software package. The EIS experiments were performed using the same apparatus in conjunction with a Schlumberger SI 1255 HF frequency response analyzer controlled with the PAR Model 398 software package. To obtain comparable and reproducible results, all of the measurements were carried out using the same preparations, procedures, and conditions at 298 K. The international sign convention is used: cathodic currents and lagged-phase shifts or angles are taken as negative. All potentials are given on the standard hydrogen electrode (SHE) scale. The Gaussian and adsorption isotherm analyses were carried out using the Excel and Origin software packages.

3. Results and discussion

3.1. Theoretical and experimental backgrounds of the phase-shift method

The equivalent circuit for the adsorption of (H + D) for the cathodic (HER + DER) at the Pt–Ir alloy/0.1 M LiOH ($\text{H}_2\text{O} + \text{D}_2\text{O}$) solution interface can be expressed as shown in Fig. 1a [27, 28, 37–39]. Taking into account the superposition of various effects (e.g. a relaxation time effect, a real surface area problem, surface absorption and diffusion processes, inhomogeneous and lateral interaction effects, an oxide layer formation, specific adsorption effects, etc.) that are inevitable under the experimental conditions, we define the equivalent circuit elements as follows: R_S is the real solution resistance; R_F is the real resistance due to the faradaic resistance (R_ϕ) for the discharge step and superposition of various effects; R_P is the real resistance due to the faradaic resistance (R_R) for the recombination step and superposition of various effects; C_P is the real capacitance due to the adsorption pseudocapacitance (C_ϕ) for the discharge step and superposition of various effects; and C_D is the real double-layer capacitance. Correspondingly, neither R_F nor C_P is constant; both depend on E and θ and can be measured. Note that both R_ϕ and C_ϕ also depend on E and θ but cannot be measured.

The numerical derivation of C_ϕ from the Frumkin and Langmuir adsorption isotherms (θ vs. E) is described elsewhere, and R_ϕ depends on C_ϕ [37,39]. A unique feature of R_ϕ and C_ϕ is that they attain maximum values at $\theta \approx 0.5$ and intermediate E , decrease symmetrically with E at other values of θ , and approach minimum values or 0 at $\theta \approx 0$ and low E and $\theta \approx 1$ and high E ; this behavior is well known in interfacial electrochemistry, electrode kinetics, and EIS. The unique feature and combination of R_ϕ and C_ϕ vs. E imply that the normalized rate of change of $-\varphi$ with respect to E , i.e. $\Delta(-\varphi)/\Delta E$, corresponds to that of θ vs. E , i.e. $\Delta\theta/\Delta E$, and vice versa (see footnotes in Table 1). Both $\Delta(-\varphi)/\Delta E$ and $\Delta\theta/\Delta E$ are maximized at $\theta \approx 0.5$ and intermediate E , decrease symmetrically with E at other values of θ , and are minimized at $\theta \approx 0$ and low E and $\theta \approx 1$ and high E . Notably, this is not a mere coincidence but rather a unique feature of the Frumkin and Langmuir adsorption isotherms (θ vs. E). The linear relationship between and Gaussian profiles of $-\varphi$ vs. E or $\Delta(-\varphi)/\Delta E$ and θ vs. E or $\Delta\theta/\Delta E$ most clearly appear at f_o . The value of f_o is experimentally and graphically evaluated on the basis of $\Delta(-\varphi)/\Delta E$ and $\Delta\theta/\Delta E$ for intermediate and other frequencies (see Figs. 3 to 5). The importance of f_o is described elsewhere [21]. These aspects are the essential nature of the phase-shift method for determining the Frumkin and Langmuir adsorption isotherms.

The frequency responses of the equivalent circuit for all f that is shown in Fig. 1a are essential for understanding the unique feature and combination of (R_S, R_F) and (C_P, C_D) vs. E for f_o , i.e. the linear relationship between the $-\varphi$ vs. E behavior for f_o and the θ vs. E behavior. At intermediate frequencies, one finds regions in which the equivalent circuit for all f behaves as a series circuit of R_S, R_F , and C_P or a series and parallel circuit of R_S, C_P , and C_D , as shown in Fig. 1 b. However, note that the simplified equivalent circuits shown in Fig. 1b do not represent the change of the cathodic (HER + DER) itself but only the intermediate frequency responses.

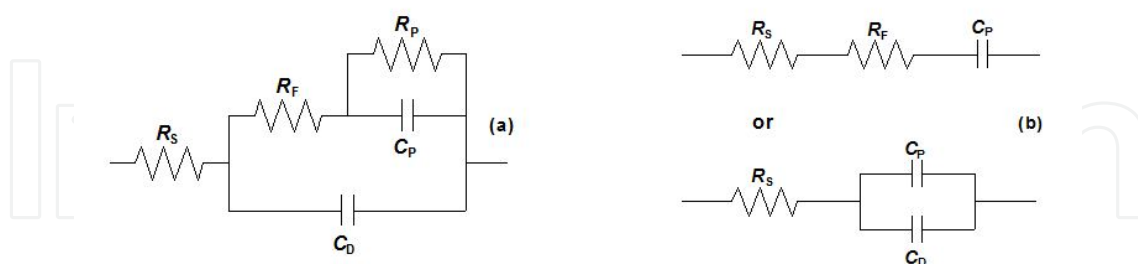


Figure 1. (a) Experimentally proposed equivalent circuit for the phase-shift method. (b) Simplified equivalent circuits for intermediate frequency responses.

At intermediate frequencies, the impedance (Z) and lagged phase-shift ($-\varphi$) are given by [27–29]

$$Z = R_S + R_F - (j / \omega C_P) \tag{1a}$$

$$-\varphi = \arctan [1 / \omega(R_S + R_F)C_P] \quad (1b)$$

for the upper circuit in Fig. 1b or

$$Z = R_S - [j / \omega(C_P + C_D)] \quad (2a)$$

$$-\varphi = \arctan [1 / \omega R_S (C_P + C_D)] \quad (2b)$$

for the lower circuit in Fig. 1b, where j is the imaginary unit (i.e. $j^2 = -1$) and ω is the angular frequency, defined as $\omega = 2\pi f$, where f is the frequency. Under these conditions,

$$R_p \gg 1 / \omega C_p \text{ and } R_p \gg R_S + R_F \quad (3)$$

In our previous papers [9–24], only Eq. (1) was used with a footnote stating that C_P practically includes C_D (see Tables 1 and 2 in Ref. 20, Table 1 in Ref. 19, etc.). Both Eqs. (1) and (2) show that the effect of R_p on $-\varphi$ for intermediate frequencies is negligible. These aspects are completely overlooked, confused, and misunderstood in the comments on the phase-shift method by Horvat-Radosevic et al. [30,32,34]. Correspondingly, all of the simulations of the phase-shift method using Eq. (1) that appear in these comments (where C_P does not include C_D) [30,32,34] are basically invalid or wrong [27,28]. All of the analyses of the effect of R_p on $-\varphi$ for intermediate frequencies are also invalid or wrong (see Supporting Information of Refs. 27 and 28).

The following limitations and conditions of the equivalent circuit elements for f_o are summarized on the basis of the experimental data in our previous papers [9–29]. Neither R_S nor C_D is constant. At $\theta \approx 0$, $R_S > R_F$ and $C_D > C_P$, or vice versa, and so forth. For a wide range of θ (i.e. $0.2 < \theta < 0.8$), $R_F \gg R_S$ or $R_F > R_S$ and $C_P \gg C_D$ or $C_P > C_D$, and so forth. At $\theta \approx 1$, $R_S > R_F$ or $R_S < R_F$ and $C_P \gg C_D$. The measured $-\varphi$ for f_o depends on E and θ . In contrast to the numerical simulations, the limitations and conditions for Eq. (1) or (2) are not considered for the phase-shift method because all of the measured values of $-\varphi$ for intermediate frequencies include (R_S, R_F) and (C_P, C_D) . Correspondingly, the measured $-\varphi$ for f_o is valid and correct regardless of the applicability of Eq. (1) or (2). Both the measured values of $-\varphi$ at f_o and the calculated values of $-\varphi$ at f_o using Eq. (1) or (2) are exactly the same (see Supporting Information in Refs. 27 and 28). The unique feature and combination of (R_S, R_F) and (C_P, C_D) are equivalent to those of R_ϕ and C_ϕ . This is attributed to the reciprocal property of R_F and C_P vs. E and suggests that only the polar form of the equivalent circuit impedance, i.e. $-\varphi$ described in Eq. (1b) or (2b), is useful and effective for studying the linear relationship between the $-\varphi$ ($90^\circ \geq -\varphi \geq 0^\circ$) vs. E behavior at f_o and the θ ($0 \leq \theta \leq 1$) vs. E behavior. Note that the phase-shift method for determining the electrochemical (Frumkin, Langmuir, Temkin) adsorption isotherms has been proposed and verified on the basis of the phase-shift curves ($-\varphi$

vs. $\log f$) at various E (see Fig. 2). The unique feature and combination of (R_S, R_F) and (C_P, C_D) vs. E , i.e. $-\varphi$ vs. E or $\Delta(-\varphi)/\Delta E$ and θ vs. E or $\Delta\theta/\Delta E$, most clearly appear at f_0 . The linear relationship between and Gaussian profiles of $-\varphi$ vs. E or $\Delta(-\varphi)/\Delta E$ and θ vs. E or $\Delta\theta/\Delta E$ for f_0 imply that only one Frumkin or Langmuir adsorption isotherm is determined on the basis of relevant experimental results (see Figs. 3 to 5). The shape and location of the $-\varphi$ vs. E or $\Delta(-\varphi)/\Delta E$ profile for f_0 and the θ vs. E or $\Delta\theta/\Delta E$ profile correspond to the interaction parameter (g) and equilibrium constant (K_0) for the Frumkin or Langmuir adsorption isotherm, respectively. These aspects have been experimentally and consistently verified or confirmed in our previous papers [9–29].

3.2. Basic procedure and description of the phase-shift method

Note that the following description of the phase-shift method for determining the Frumkin adsorption isotherm is similar to our previous papers due to use of the same method and procedures [27,28].

Figure 2 compares the phase-shift curves ($-\varphi$ vs. $\log f$) for different E at the Pt–Ir alloy/0.1 M LiOH ($H_2O + D_2O$) solution interface. As shown in Fig. 2, $-\varphi$ depends on both f and E [37–39]. Correspondingly, the normalized rate of change of $-\varphi$ vs. E , i.e. $\Delta(-\varphi)/\Delta E$, depends on both f and E . In electrosorption, θ depends on only E [40]. The normalized rate of change of θ vs. E , i.e. $\Delta\theta/\Delta E$, obeys a Gaussian profile. This is a unique feature of the Frumkin and Langmuir adsorption isotherms (θ vs. E).

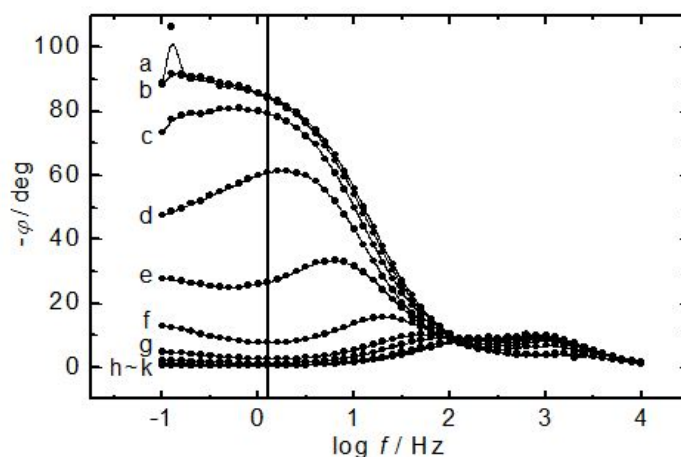


Figure 2. Comparison of the phase-shift curves ($-\varphi$ vs. $\log f$) for different potentials (E) at the Pt–Ir alloy/0.1 M LiOH ($H_2O + D_2O$) solution interface. Measured values: ●. Vertical solid line: 1.259 Hz; single sine wave; scan frequency range, (10^4 to 0.1) Hz; ac amplitude, 5 mV. Dc potentials: (a) -0.659 V, (b) -0.684 V, (c) -0.709 V, (d) -0.734 V, (e) -0.759 V, (f) -0.784 V, (g) -0.809 V, (h) -0.834 V, (i) -0.859 V, (j) -0.884 V, and (k) -0.909 V (all vs. SHE).

The intermediate frequency of 1.259 Hz, shown as a vertical solid line on the $-\varphi$ vs. $\log f$ plot in Fig. 2, can be set as f_0 for $-\varphi$ vs. E and θ vs. E profiles. The determination of f_0 is experimentally and graphically evaluated on the basis of $\Delta(-\varphi)/\Delta E$ and $\Delta\theta/\Delta E$ for intermediate

and other frequencies (see Figs. 3 and 4). At the maximum $-\varphi$ shown in curve a of Fig. 2, it appears that the adsorption of (H + D) and superposition of various effects are minimized; i.e. $\theta \approx 0$ and E is low. Note that θ ($0 \leq \theta \leq 1$) depends only on E . At the maximum $-\varphi$, when $\theta \approx 0$ and E is low, both $\Delta(-\varphi)/\Delta E$ and $\Delta\theta/\Delta E$ are minimized because R_ϕ and C_ϕ approach minimum values or 0. At the minimum $-\varphi$, shown in curve k of Fig. 2, it appears that the adsorption of (H + D) and superposition of various effects are maximized or almost saturated; i.e. $\theta \approx 1$ and E is high. At the minimum $-\varphi$, when $\theta \approx 1$ and E is high, both $\Delta(-\varphi)/\Delta E$ and $\Delta\theta/\Delta E$ are also minimized because R_ϕ and C_ϕ approach minimum values or 0. At the medium $-\varphi$ between curves d and e in Fig. 2, it appears that both $\Delta(-\varphi)/\Delta E$ and $\Delta\theta/\Delta E$ are maximized because R_ϕ and C_ϕ approach maximum values at $\theta \approx 0.5$ and intermediate E (see Table 1 and Fig. 4b). If one knows the three points or regions, i.e. the maximum $-\varphi$ ($\theta \approx 0$ and low E region, where $\Delta(-\varphi)/\Delta E$ and $\Delta\theta/\Delta E$ approach the minimum value or 0), the medium $-\varphi$ ($\theta \approx 0.5$ and intermediate E region, where $\Delta(-\varphi)/\Delta E$ and $\Delta\theta/\Delta E$ approach the maximum value), and the minimum $-\varphi$ ($\theta \approx 1$ and high E region, where $\Delta(-\varphi)/\Delta E$ and $\Delta\theta/\Delta E$ approach the minimum value or 0) for f_o , then one can easily determine the object, i.e. the Frumkin or Langmuir adsorption isotherm. In other words, both $\Delta(-\varphi)/\Delta E$ and $\Delta\theta/\Delta E$ for f_o are maximized at $\theta \approx 0.5$ and intermediate E , decrease symmetrically with E at other values of θ , and are minimized at $\theta \approx 0$ and low E and $\theta \approx 1$ and high E (see Table 1 and Fig. 4b). As stated above, this is a unique feature of the Frumkin and Langmuir adsorption isotherms. The linear relationship between and Gaussian profiles of $-\varphi$ vs. E or $\Delta(-\varphi)/\Delta E$ and θ vs. E or $\Delta\theta/\Delta E$ most clearly appear at f_o .

E/V vs. SHE	$-\varphi/\text{deg}$	θ^a	$\Delta(-\varphi)/\Delta E^b$	$\Delta\theta/\Delta E^c$
-0.659	84.7	~ 0	~ 0	~ 0
-0.684	84.0	0.00830	0.08304	0.08304
-0.709	79.4	0.06287	0.54567	0.54567
-0.734	60.8	0.28351	2.20641	2.20641
-0.759	26.6	0.68921	4.05694	4.05694
-0.784	7.7	0.91340	2.24199	2.24199
-0.809	2.6	0.97390	0.60498	0.60498
-0.834	1.3	0.98932	0.15421	0.15421
-0.859	0.7	0.99644	0.07117	0.07117
-0.884	0.6	0.99763	0.01186	0.01186
-0.909	0.4	~ 1	0.02372	0.02372

Table 1. ^a ($0 \leq \theta \leq 1$) and estimated using $-\varphi$. ^b $\{[(\text{neighbor phase shift difference})/(\text{total phase shift difference})]/[(\text{neighbor potential difference})/(\text{total potential difference})]\}$. ^c $\{[(\text{neighbor fractional surface coverage difference})/(\text{total fractional surface coverage difference})]/[(\text{neighbor potential difference})/(\text{total potential difference})]\}$. Measured values of the phase shift ($-\varphi$) for the optimum intermediate frequency ($f_o = 1.259$ Hz), the fractional surface coverage (θ) of (H + D), and the normalized rates of change of $-\varphi$ and θ vs. E (i.e. $\Delta(-\varphi)/\Delta E$, $\Delta\theta/\Delta E$) at the Pt-Ir alloy/0.1 M LiOH ($\text{H}_2\text{O} + \text{D}_2\text{O}$) solution interface

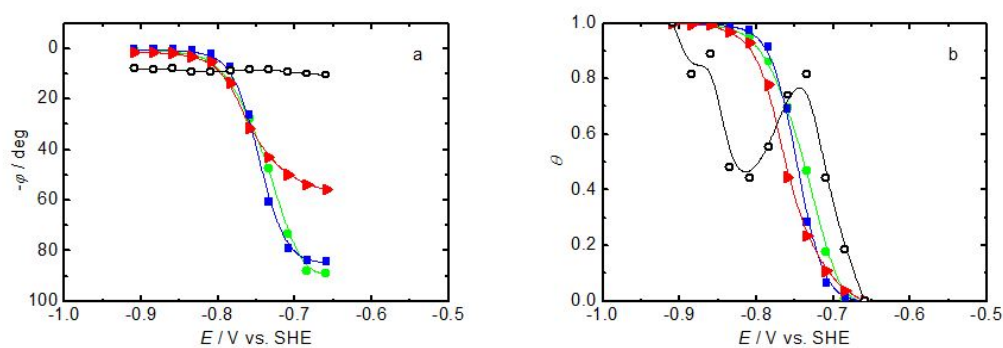


Figure 3. Comparison of (a) the phase-shift profiles ($-\varphi$ vs. E) and (b) the fractional surface coverage profiles (θ vs. E) for four different frequencies at the Pt-Ir alloy/0.1 M LiOH ($\text{H}_2\text{O} + \text{D}_2\text{O}$) solution interface. Measured or estimated values: ●, 0.1 Hz; ■, 1.259 Hz; ►, 10 Hz; ○, 100 Hz. The optimum intermediate frequency (f_0) is 1.259 Hz.

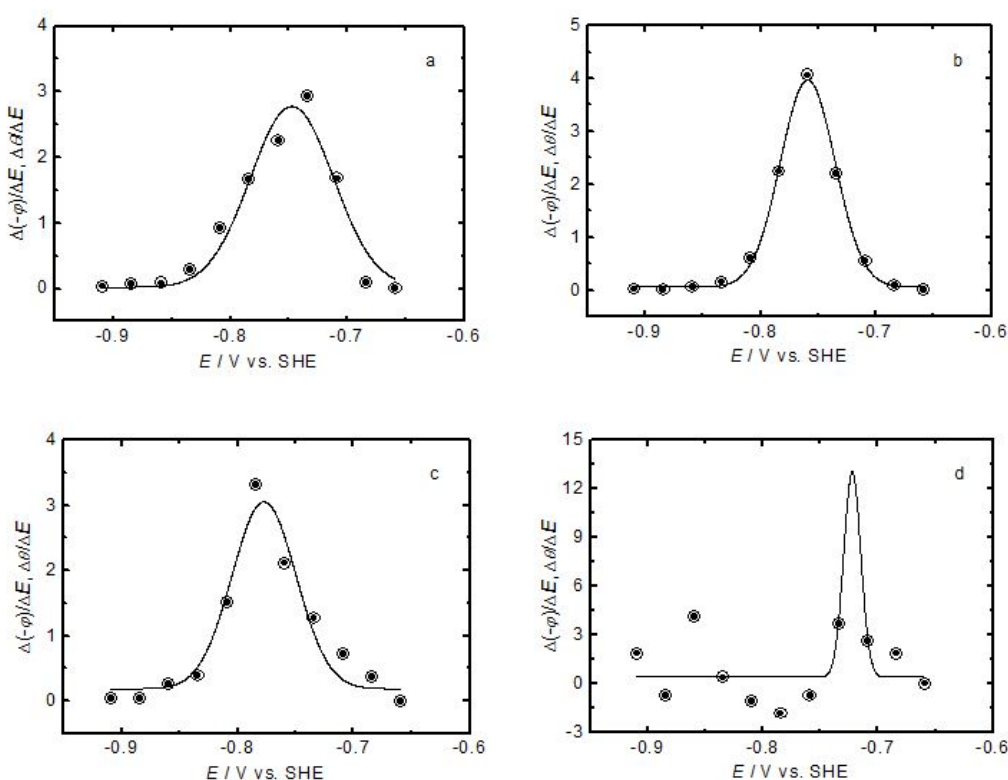


Figure 4. Comparison of the normalized rates of change of $-\varphi$ and θ vs. E , i.e. $\Delta(-\varphi)/\Delta E$ and $\Delta\theta/\Delta E$, for four different frequencies at the Pt-Ir alloy/0.1 M LiOH ($\text{H}_2\text{O} + \text{D}_2\text{O}$) solution interface. Solid curves show the fitted Gaussian profiles. Measured or estimated values: ○, $\Delta(-\varphi)/\Delta E$; ●, $\Delta\theta/\Delta E$. (a) 0.1 Hz, (b) 1.259 Hz, (c) 10 Hz, and (d) 100 Hz. The optimum intermediate frequency (f_0) is 1.259 Hz.

The procedure and description of the phase-shift method for determining the Frumkin adsorption isotherm of (H + D) at the interface are summarized in Table 1. The values of $-\varphi$ and θ as a function of E at $f_0 = 1.259$ Hz shown in Fig. 3 are illustrated on the basis of the experimental results summarized in Table 1. The values of $-\varphi$ and θ as a function of E at $f =$

0.1 Hz, 10 Hz, and 100 Hz shown in Fig. 3 are also illustrated through the same procedure summarized in Table 1. However, note that the differences between the $-\varphi$ vs. E profile at $f_0 = 1.259$ Hz and the $-\varphi$ vs. E profiles at $f = 0.1$ Hz, 10 Hz, and 100 Hz shown in Fig. 3a do not represent the measurement error but only the frequency response. In practice, the θ vs. E profiles at $f = 0.1$ Hz, 10 Hz, and 100 Hz shown in Fig. 3b should be exactly the same as the θ vs. E profile at $f_0 = 1.259$ Hz. Because, as stated above, θ depends on only E and this unique feature most clearly appears at f_0 . This is the reason why the comparison of $-\varphi$ and θ vs. E profiles for different frequencies shown in Fig. 3 is necessary to determine f_0 .

The Gaussian profile shown in Fig. 4b is illustrated on the basis of $\Delta(-\varphi)/\Delta E$ and $\Delta\theta/\Delta E$ data for $f_0 = 1.259$ Hz summarized in Table 1. Figure 4b shows that both $\Delta(-\varphi)/\Delta E$ and $\Delta\theta/\Delta E$ are maximized at $\theta \approx 0.5$ and intermediate E , decrease symmetrically with E at other values of θ , and are minimized at $\theta \approx 0$ and low E and $\theta \approx 1$ and high E . The Gaussian profiles for $f = 0.1$ Hz, 10 Hz, and 100 Hz shown in Fig. 4 were obtained through the same procedure summarized in Table 1. Finally, one can conclude that the θ vs. E profile at $f_0 = 1.259$ Hz shown in Fig. 3b is applicable to the determination of the Frumkin adsorption isotherm of (H + D) at the interface. As stated above, the shape and location of the $-\varphi$ vs. E or $\Delta(-\varphi)/\Delta E$ profile and the θ vs. E or $\Delta\theta/\Delta E$ profile for f_0 correspond to g and K_0 for the Frumkin adsorption isotherm, respectively.

3.3. Frumkin, Langmuir, and Temkin adsorption isotherms

The derivation and interpretation of the practical forms of the electrochemical Frumkin, Langmuir, and Temkin adsorption isotherms are described elsewhere [41–43]. The Frumkin adsorption isotherm assumes that the Pt–Ir alloy surface is inhomogeneous or that the lateral interaction effect is not negligible. It is well known that the Langmuir adsorption isotherm is a special case of the Frumkin adsorption isotherm. The Langmuir adsorption isotherm can be derived from the Frumkin adsorption isotherm by setting the interaction parameter to be zero. The Frumkin adsorption isotherm of (H + D) can be expressed as follows [42]

$$[\theta / (1 - \theta)] \exp(g\theta) = K_0 C^+ \exp(-EF / RT) \quad (4)$$

$$g = r / RT \quad (5)$$

$$K = K_0 \exp(-g\theta) \quad (6)$$

where θ ($0 \leq \theta \leq 1$) is the fractional surface coverage, g is the interaction parameter for the Frumkin adsorption isotherm, K_0 is the equilibrium constant at $g = 0$, C^+ is the concentration of ions (H^+ , D^+) in the bulk solution, E is the negative potential, F is Faraday's constant, R is the gas constant, T is the absolute temperature, r is the rate of change of the standard Gibbs energy of (H + D) adsorption with θ , and K is the equilibrium constant. The dimension of K is described elsewhere [44]. Note that when $g = 0$ in Eqs. (4) to (6), the Langmuir adsorption

isotherm is obtained. For the Langmuir adsorption isotherm, when $g = 0$, the inhomogeneous and lateral interaction effects on the adsorption of (H + D) are assumed to be negligible.

At the Pt-Ir alloy/0.1 M LiOH (H₂O + D₂O) solution interface, the numerically calculated Frumkin adsorption isotherms using Eq. (4) are shown in Fig. 5. Curves a, b, and c in Fig. 5 show the three numerically calculated Frumkin adsorption isotherms of (H + D) corresponding to $g = 0, -2.2,$ and $-5.5,$ respectively, for $K_0 = 5.3 \times 10^{-5} \text{ mol}^{-1}$. The curve b shows that the Frumkin adsorption isotherm, $K = 5.3 \times 10^{-5} \exp(2.2\theta) \text{ mol}^{-1}$, is applicable to the adsorption of (H + D), and Eq. (5) gives $r = -5.5 \text{ kJ} \cdot \text{mol}^{-1}$. The Frumkin adsorption isotherm implies that the lateral interaction between the adsorbed (H + D) species is not negligible. In other words, the Langmuir adsorption isotherm for $g = 0$, i.e. $K = 5.3 \times 10^{-5} \text{ mol}^{-1}$, is not applicable to the adsorption of (H + D) at the interface (see Fig. 8).

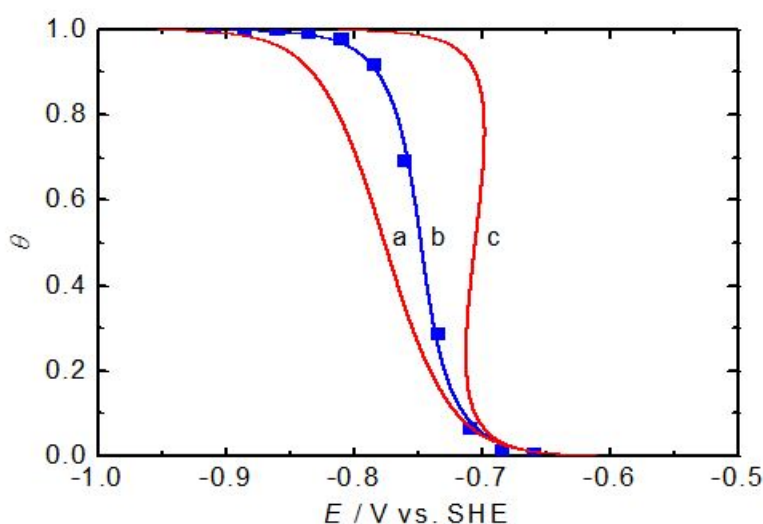


Figure 5. Comparison of the experimental and fitted data for the Frumkin adsorption isotherms of (H + D) at the Pt-Ir alloy/0.1 M LiOH (H₂O + D₂O) solution interface. Experimental data: ■. Curves show the Frumkin adsorption isotherms calculated using Eq. (4) for (a) $g = 0$, (b) $g = -2.2$, and (c) $g = -5.5$ with $K_0 = 5.3 \times 10^{-5} \text{ mol}^{-1}$.

At intermediate values of θ (i.e. $0.2 < \theta < 0.8$), the pre-exponential term, $[\theta/(1 - \theta)]$, varies little with θ in comparison with the variation of the exponential term, $\exp(g\theta)$. Under these approximate conditions, the Temkin adsorption isotherm can be simply derived from the Frumkin adsorption isotherm. The Temkin adsorption isotherm of (H + D) can be expressed as follows [42]

$$\exp(g\theta) = K_0 C^+ \exp(-EF / RT) \quad (7)$$

Figure 6 shows the determination of the Temkin adsorption isotherm corresponding to the Frumkin adsorption isotherm shown in curve b of Fig. 5. The dashed line labeled b in Fig. 6

shows that the numerically calculated Temkin adsorption isotherm of (H + D) using Eq. (7) is $K = 5.3 \times 10^{-4} \exp(-2.4\theta) \text{ mol}^{-1}$, and Eq. (5) gives $r = 6.0 \text{ kJ} \cdot \text{mol}^{-1}$. The values of g and K for the Frumkin and Temkin adsorption isotherms of H, D, (H + D), OH, and (OH + OD) at the noble and highly corrosion-resistant metal and alloy/H₂O and D₂O solution interfaces are summarized in Tables 2 and 3, respectively.

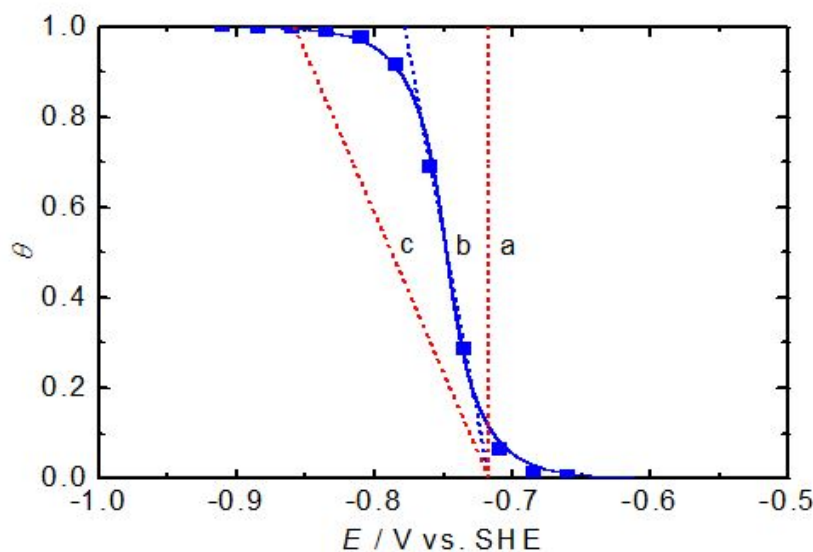


Figure 6. Comparison of the experimentally determined Frumkin adsorption isotherm and three fitted Temkin adsorption isotherms of (H + D) at the Pt–Ir alloy/0.1 M LiOH (H₂O + D₂O) solution interface. Experimental data: ■. The curve shows the Frumkin adsorption isotherm calculated using Eq. (4). Dashed lines show the Temkin adsorption isotherms calculated using Eq. (7) and the correlation constants for (a) $g = 0$, (b) $g = 2.4$, and (c) $g = 5.5$ with $K_0 = 5.3 \times 10^{-4} \text{ mol}^{-1}$.

3.4. Applicability of the Frumkin, Langmuir, and Temkin adsorption isotherms

Figure 7 shows the applicability of ranges of θ , which are estimated using the measured phase shift ($-\varphi$) shown in Table 1, for the Frumkin adsorption isotherm at the Pt–Ir alloy/0.1 M LiOH (H₂O + D₂O) solution interface. Fig. 7 also shows that the phase-shift method for determining the Frumkin adsorption isotherm (θ vs. E) is valid, effective, and reasonable at $0 \leq \theta \leq 1$.

Figures 8 and 9 show the applicability of the Langmuir and Temkin adsorption isotherms at the same potential ranges, respectively. Figs. 8 and 9 also show that the Langmuir and Temkin adsorption isotherms are not applicable to the adsorption of (H + D) at the interface.

At extreme values of θ , i.e. $\theta \approx 0$ and 1, the Langmuir adsorption isotherm is often applicable to the adsorption of intermediates [42]. However, as shown in Figs. 8b and c, the validity and correctness of the Langmuir adsorption isotherm are unclear and limited even at $\theta \approx 0$ and 1. As stated in the introduction, the value of g for the Frumkin adsorption isotherm is not experimentally and consistently determined using other conventional methods. This is the reason why the Langmuir adsorption isotherm is often used even though it has the criti-

cal limitation and applicability. On the other hand, the Temkin adsorption isotherm is only valid and effective at $0.2 < \theta < 0.8$ (see Fig. 6). Note that the short potential range (ca. 37 mV) is difficult to observe in the Temkin adsorption isotherm correlating with the Frumkin adsorption isotherm. At other values of θ , i.e. $0 \leq \theta < 0.2$ and $0.8 < \theta \leq 1$, only the Frumkin adsorption isotherm is applicable to the adsorption of (H + D). Finally, one can conclude that the Frumkin adsorption isotherm is more useful, effective, and reliable than the Langmuir and Temkin adsorption isotherms at the interface.

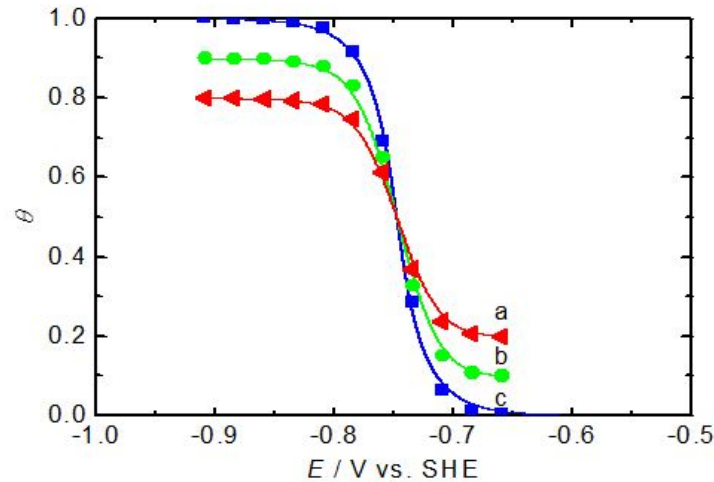


Figure 7. Comparison of ranges of θ for the Frumkin adsorption isotherm of (H + D) at the Pt-Ir alloy/0.1 M LiOH ($H_2O + D_2O$) solution interface. (a) $0.2 < \theta < 0.8$ (\blacktriangle), (b) $0.1 < \theta < 0.9$ (\bullet), and (c) $0 \leq \theta \leq 1$ (\blacksquare). The blue curve is the Frumkin adsorption isotherm, $K = 5.3 \times 10^{-5} \exp(2.2\theta) \text{ mol}^{-1}$.

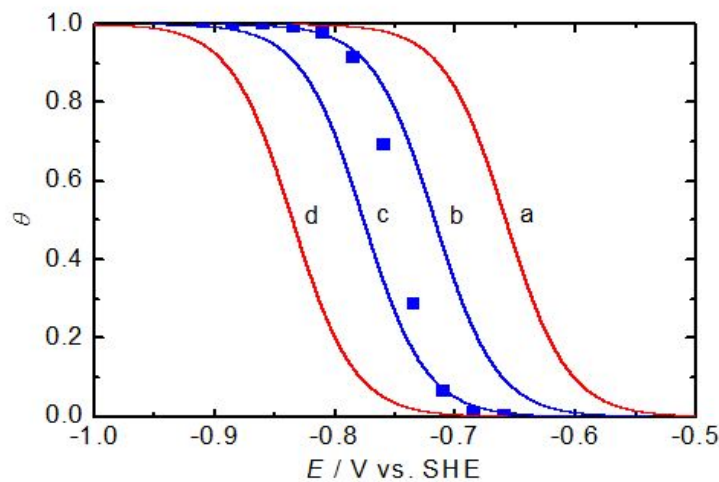


Figure 8. Comparison of the Langmuir adsorption isotherms of (H + D) at the same potential ranges. Experimental data: \blacksquare . Curves show the Langmuir adsorption isotherms (θ vs. E) calculated using Eq. (4) for $g = 0$. (a) $K = 5.3 \times 10^{-3} \text{ mol}^{-1}$, (b) $K = 5.3 \times 10^{-4} \text{ mol}^{-1}$, (c) $K = 5.3 \times 10^{-5} \text{ mol}^{-1}$, and (d) $K = 5.3 \times 10^{-6} \text{ mol}^{-1}$.

interface	adsorbate	g	K/mol^{-1}	Ref.
Pt-Ir alloy ^a /0.1 M LiOH (H ₂ O+D ₂ O)	H+D	-2.2	$5.3 \times 10^{-5} \exp(2.2\theta)$	-
Pt-Ir alloy ^a /0.1 M LiOH (H ₂ O)	H	-2.2	$8.6 \times 10^{-5} \exp(2.2\theta)$	27
Pt-Ir alloy ^a /0.1 M LiOH (D ₂ O)	D	-2.3	$2.1 \times 10^{-5} \exp(2.3\theta)$	27
Pt-Ir alloy ^a /0.5 M H ₂ SO ₄ (H ₂ O)	H	-2.5	$3.3 \times 10^{-5} \exp(2.5\theta)$	28
Pt-Ir alloy ^a /0.1 M LiOH (H ₂ O)	OH	0.6	$5.4 \times 10^{-9} \exp(-0.6\theta)$	26
Pt-Ir alloy ^a /0.1 M LiOH (D ₂ O)	OH+OD	2.7	$3.9 \times 10^{-9} \exp(-2.7\theta)$	26
Pt-Ir alloy ^b /0.5 M H ₂ SO ₄ (H ₂ O)	H	-2.5	$3.1 \times 10^{-5} \exp(2.5\theta)$	20
Pt-Ir alloy ^b /0.1 M KOH (H ₂ O)	OH	1.8	$4.7 \times 10^{-10} \exp(-1.8\theta)$	20
Pt/0.1 M KOH (H ₂ O)	H	-2.4	$1.2 \times 10^{-4} \exp(2.4\theta)$	25
Pt/0.5 M H ₂ SO ₄ (H ₂ O)	H	-2.4	$3.5 \times 10^{-5} \exp(2.4\theta)$	21
Ir/0.1 M KOH (H ₂ O)	H	-2.4	$9.4 \times 10^{-5} \exp(2.4\theta)$	25
Ir/0.5 M H ₂ SO ₄ (H ₂ O)	H	-2.4	$2.7 \times 10^{-5} \exp(2.4\theta)$	21
Pd/0.5 M H ₂ SO ₄ (H ₂ O)	H	1.4	$3.3 \times 10^{-5} \exp(-1.4\theta)$	19
Au/0.5 M H ₂ SO ₄ (H ₂ O)	H	0 ^e	2.3×10^{-6}	13
Re/0.1 M KOH (H ₂ O)	H	0 ^e	1.9×10^{-6}	16
Re/0.5 M H ₂ SO ₄ (H ₂ O)	H	0 ^e	4.5×10^{-7}	16
Ni ^c /0.05 M KOH (H ₂ O)	H	10	$1.3 \times 10^{-1} \exp(-10\theta)$	11
Ni ^d /0.1 M LiOH (H ₂ O)	H	7.4	$3.6 \times 10^{-4} \exp(-7.4\theta)$	29
Ni ^d /0.5 M H ₂ SO ₄ (H ₂ O)	H	5.3	$4.1 \times 10^{-9} \exp(-5.3\theta)$	29
Ti/0.5 M H ₂ SO ₄ (H ₂ O)	H	6.6	$8.3 \times 10^{-12} \exp(-6.6\theta)$	23
Zr/0.2 M H ₂ SO ₄ (H ₂ O)	H	3.5	$1.4 \times 10^{-17} \exp(-3.5\theta)$	24

Table 2. ^a Pt-Ir (90:10 mass ratio) alloy. ^b Pt-Ir (70:30 mass ratio) alloy. ^c Ni (purity 99.994%) foil. ^d Ni (purity 99.999%) wire. ^e Langmuir adsorption isotherm. Comparison of the interaction parameters (g) and equilibrium constants (K) for the Frumkin adsorption isotherms at the noble and highly corrosion-resistant metal and alloy/H₂O and D₂O solution interfaces

interface	adsorbate	g	K/mol^{-1}	Ref.
Pt-Ir alloy ^a /0.1 M LiOH (H ₂ O+D ₂ O)	H+D	2.4	$5.3 \times 10^{-4} \exp(-2.4\theta)$	-
Pt-Ir alloy ^a /0.1 M LiOH (H ₂ O)	H	2.4	$8.6 \times 10^{-4} \exp(-2.4\theta)$	27
Pt-Ir alloy ^a /0.1 M LiOH (D ₂ O)	D	2.3	$2.1 \times 10^{-4} \exp(-2.3\theta)$	27
Pt-Ir alloy ^a /0.5 M H ₂ SO ₄ (H ₂ O)	H	2.1	$3.3 \times 10^{-4} \exp(-2.1\theta)$	28
Pt-Ir alloy ^a /0.1 M LiOH (H ₂ O)	OH	5.2	$5.4 \times 10^{-8} \exp(-5.2\theta)$	26
Pt-Ir alloy ^a /0.1 M LiOH (D ₂ O)	OH+OD	7.3	$3.9 \times 10^{-8} \exp(-7.3\theta)$	26

Pt-Ir alloy ^b /0.5 M H ₂ SO ₄ (H ₂ O)	H	2.1	$3.1 \times 10^{-4} \exp(-2.1\theta)$	20
Pt-Ir alloy ^b /0.1 M KOH (H ₂ O)	OH	6.4	$4.7 \times 10^{-9} \exp(-6.4\theta)$	20
Pt/0.1 M KOH (H ₂ O)	H	2.2	$1.2 \times 10^{-3} \exp(-2.2\theta)$	25
Pt/0.5 M H ₂ SO ₄ (H ₂ O)	H	2.2	$3.5 \times 10^{-4} \exp(-2.2\theta)$	21
Ir/0.1 M KOH (H ₂ O)	H	2.2	$9.4 \times 10^{-4} \exp(-2.2\theta)$	25
Ir/0.5 M H ₂ SO ₄ (H ₂ O)	H	2.2	$2.7 \times 10^{-4} \exp(-2.2\theta)$	21
Pd/0.5 M H ₂ SO ₄ (H ₂ O)	H	6	$3.3 \times 10^{-4} \exp(-6\theta)$	19
Au/0.5 M H ₂ SO ₄ (H ₂ O)	H	4.6	$2.3 \times 10^{-5} \exp(-4.6\theta)$	13
Re/0.1 M KOH (H ₂ O)	H	4.6	$1.9 \times 10^{-5} \exp(-4.6\theta)$	16
Re/0.5 M H ₂ SO ₄ (H ₂ O)	H	4.6	$4.5 \times 10^{-6} \exp(-4.6\theta)$	16
Ni ^c /0.05 M KOH (H ₂ O)	H	14.6	$1.3 \exp(-14.6\theta)$	11
Ni ^d /0.1 M LiOH (H ₂ O)	H	12	$3.6 \times 10^{-3} \exp(-12\theta)$	29
Ni ^d /0.5 M H ₂ SO ₄ (H ₂ O)	H	9.9	$4.1 \times 10^{-8} \exp(-9.9\theta)$	29
Ti/0.5 M H ₂ SO ₄ (H ₂ O)	H	11.2	$8.3 \times 10^{-11} \exp(-11.2\theta)$	23
Zr/0.2 M H ₂ SO ₄ (H ₂ O)	H	8.1	$1.4 \times 10^{-16} \exp(-8.1\theta)$	24

Table 3. ^a Pt-Ir (90:10 mass ratio) alloy. ^b Pt-Ir (70:30 mass ratio) alloy. ^c Ni (purity 99.994%) foil. ^d Ni (purity 99.999%) wire. Comparison of the interaction parameters (g) and equilibrium constants (K) for the Temkin adsorption isotherms at the noble and highly corrosion-resistant metal and alloy/H₂O and D₂O solution interfaces

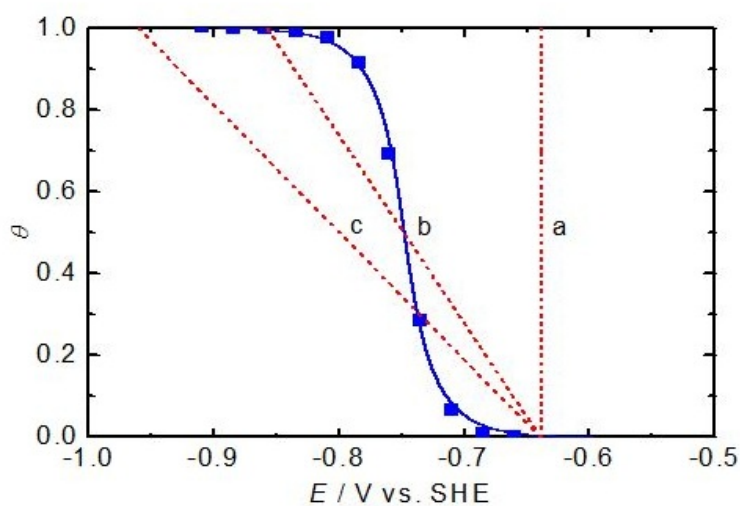


Figure 9. Comparison of the Temkin adsorption isotherms of (H + D) at the same potential ranges. Experimental data: ■. The curve shows the Frumkin adsorption isotherm calculated using Eq. (4). Dashed lines show the Temkin adsorption isotherms calculated using Eq. (7) for (a) $g = 0$, (b) $g = 8.5$, and (c) $g = 12.5$ with $K_0 = 1.1 \times 10^{-2} \text{ mol}^{-1}$.

3.5. Standard Gibbs energy of adsorption

Under the Frumkin adsorption conditions, the relationship between the equilibrium constant (K) for (H + D) and the standard Gibbs energy ($\Delta G_{\theta}^{\circ}$) of (H + D) adsorption is [42]

$$2.3RT \log K = -\Delta G_{\theta}^{\circ} \quad (8)$$

For the Pt–Ir alloy/0.1 M LiOH (H₂O + D₂O) solution interface, use of Eqs. (6) and (8) shows that $\Delta G_{\theta}^{\circ}$ is in the range ($24.4 \geq \Delta G_{\theta}^{\circ} \geq 18.9$) kJ · mol⁻¹ for $K = 5.3 \times 10^{-5} \exp(2.2\theta)$ mol⁻¹ and $0 \leq \theta \leq 1$. This result implies an increase in the absolute value of $\Delta G_{\theta}^{\circ}$, i.e. $|\Delta G_{\theta}^{\circ}|$, with θ . Note that $\Delta G_{\theta}^{\circ}$ is a negative number, i.e. $\Delta G_{\theta}^{\circ} < 0$ [42]. The values of $\Delta G_{\theta}^{\circ}$ and r for the Frumkin and Temkin adsorption isotherms at the noble and highly corrosion-resistant metal and alloy/H₂O and D₂O solution interfaces are summarized in Tables 4 and 5, respectively.

4. Comparisons

4.1. Mixture solution

Curves a, b, and c in Fig. 10 show the K vs. θ behaviors of H, (H + D), and D at the Pt–Ir alloy/0.1 M LiOH (H₂O), 0.1 M LiOH (H₂O + D₂O), and 0.1 M LiOH (D₂O) solution interfaces, respectively [27]. In Fig. 10, the value of K for (H + D) is approximately equal to the average value of K for H and D isotopes. The value of K for (H + D) decreases with increasing D₂O. In other words, the value of K decreases in going from H₂O to D₂O. Over the θ range (i.e. $1 \geq \theta \geq 0$), the value of K for H is approximately 3.7 to 4.1 times greater than that for D (see Table 2). As shown in Tables 2 and 4, the values of g , K , $\Delta G_{\theta}^{\circ}$, and r for the Frumkin adsorption isotherms of H, (H + D), and D are readily distinguishable using the phase-shift method. Fig. 10 also shows that the kinetic isotope effect, i.e. the ratio of rate constants of H and D or equilibrium constants of H and D, is readily determined using the phase-shift method (also see Table 2) [45]. Note that the kinetic isotope effect is widely used and applied in electrochemistry, surface science, biochemistry, chemical geology, physics, etc.

interface	adsorbate	$\Delta G_{\theta}^{\circ}/\text{kJ}\cdot\text{mol}^{-1}$	$r/\text{kJ}\cdot\text{mol}^{-1}$	Ref.
Pt–Ir alloy ^a /0.1 M LiOH (H ₂ O+D ₂ O)	H+D	$24.4 \geq \Delta G_{\theta}^{\circ} \geq 18.9$	-5.5	–
Pt–Ir alloy ^a /0.1 M LiOH (H ₂ O)	H	$23.2 \geq \Delta G_{\theta}^{\circ} \geq 17.7$	-5.5	27
Pt–Ir alloy ^a /0.1 M LiOH (D ₂ O)	D	$26.7 \geq \Delta G_{\theta}^{\circ} \geq 21.0$	-5.7	27
Pt–Ir alloy ^a /0.5 M H ₂ SO ₄ (H ₂ O)	H	$25.6 \geq \Delta G_{\theta}^{\circ} \geq 19.4$	-6.2	28
Pt–Ir alloy ^a /0.1 M LiOH (H ₂ O)	OH	$47.2 \leq \Delta G_{\theta}^{\circ} \leq 48.6$	1.5	26
Pt–Ir alloy ^a /0.1 M LiOH (D ₂ O)	OH+OD	$48.0 \leq \Delta G_{\theta}^{\circ} \leq 54.7$	6.7	26
Pt–Ir alloy ^b /0.5 M H ₂ SO ₄ (H ₂ O)	H	$25.7 \geq \Delta G_{\theta}^{\circ} \geq 19.5$	-6.2	20

Pt-Ir alloy ^b /0.1 M KOH (H ₂ O)	OH	$53.2 \leq \Delta G_{\theta}^{\circ} \leq 57.7$	4.5	20
Pt/0.1 M KOH (H ₂ O)	H	$22.4 \geq \Delta G_{\theta}^{\circ} \geq 16.5$	-6.0	25
Pt/0.5 M H ₂ SO ₄ (H ₂ O)	H	$25.4 \geq \Delta G_{\theta}^{\circ} \geq 19.5$	-6.0	21
Ir/0.1 M KOH (H ₂ O)	H	$23.0 \geq \Delta G_{\theta}^{\circ} \geq 17.1$	-6.0	25
Ir/0.5 M H ₂ SO ₄ (H ₂ O)	H	$26.1 \geq \Delta G_{\theta}^{\circ} \geq 20.1$	-6.0	21
Pd/0.5 M H ₂ SO ₄ (H ₂ O)	H	$25.6 \leq \Delta G_{\theta}^{\circ} \leq 29.0$	3.5	19
Au/0.5 M H ₂ SO ₄ (H ₂ O)	H	32.2	0 ^e	13
Re/0.1 M KOH (H ₂ O)	H	32.6	0 ^e	16
Re/0.5 M H ₂ SO ₄ (H ₂ O)	H	36.2	0 ^e	16
Ni ^c /0.05 M KOH (H ₂ O)	H	$5.1 \leq \Delta G_{\theta}^{\circ} \leq 29.8$	24.8	11
Ni ^d /0.1 M LiOH (H ₂ O)	H	$19.6 \leq \Delta G_{\theta}^{\circ} \leq 38.0$	18.4	29
Ni ^d /0.5 M H ₂ SO ₄ (H ₂ O)	H	$47.8 \leq \Delta G_{\theta}^{\circ} \leq 61.0$	13.1	29
Ti/0.5 M H ₂ SO ₄ (H ₂ O)	H	$63.2 \leq \Delta G_{\theta}^{\circ} \leq 79.6$	16.4	23
Zr/0.2 M H ₂ SO ₄ (H ₂ O)	H	$96.1 \leq \Delta G_{\theta}^{\circ} \leq 104.8$	8.7	24

Table 4. ^a Pt-Ir (90:10 mass ratio) alloy. ^b Pt-Ir (70:30 mass ratio) alloy. ^c Ni (purity 99.994%) foil. ^d Ni (purity 99.999%) wire. ^e Langmuir adsorption isotherm. Comparison of the standard Gibbs energies ($\Delta G_{\theta}^{\circ}$) of adsorptions and rates of change (r) of $\Delta G_{\theta}^{\circ}$ with θ ($0 \leq \theta \leq 1$) for the Frumkin adsorption isotherms at the noble and highly corrosion-resistant metal and alloy/H₂O and D₂O solution interfaces

interface	adsorbate	$\Delta G_{\theta}^{\circ}/\text{kJ}\cdot\text{mol}^{-1}$	$r/\text{kJ}\cdot\text{mol}^{-1}$	Ref.
Pt-Ir alloy ^a /0.1 M LiOH (H ₂ O+D ₂ O)	H+D	$19.9 < \Delta G_{\theta}^{\circ} < 23.4$	6.0	-
Pt-Ir alloy ^a /0.1 M LiOH (H ₂ O)	H	$18.7 < \Delta G_{\theta}^{\circ} < 22.2$	6.0	27
Pt-Ir alloy ^a /0.1 M LiOH (D ₂ O)	D	$22.2 < \Delta G_{\theta}^{\circ} < 25.6$	5.7	27
Pt-Ir alloy ^a /0.5 M H ₂ SO ₄ (H ₂ O)	H	$20.9 < \Delta G_{\theta}^{\circ} < 24.0$	5.2	28
Pt-Ir alloy ^a /0.1 M LiOH (H ₂ O)	OH	$44.0 < \Delta G_{\theta}^{\circ} < 51.8$	12.9	26
Pt-Ir alloy ^a /0.1 M LiOH (D ₂ O)	OH+OD	$45.9 < \Delta G_{\theta}^{\circ} < 56.8$	18.1	26
Pt-Ir alloy ^b /0.5 M H ₂ SO ₄ (H ₂ O)	H	$21.1 < \Delta G_{\theta}^{\circ} < 24.2$	5.2	20
Pt-Ir alloy ^b /0.1 M KOH (H ₂ O)	OH	$50.7 < \Delta G_{\theta}^{\circ} < 60.2$	15.9	20
Pt/0.1 M KOH (H ₂ O)	H	$17.8 < \Delta G_{\theta}^{\circ} < 21.0$	5.5	25
Pt/0.5 M H ₂ SO ₄ (H ₂ O)	H	$20.8 < \Delta G_{\theta}^{\circ} < 24.1$	5.5	21
Ir/0.1 M KOH (H ₂ O)	H	$18.3 < \Delta G_{\theta}^{\circ} < 21.7$	5.5	25
Ir/0.5 M H ₂ SO ₄ (H ₂ O)	H	$21.5 < \Delta G_{\theta}^{\circ} < 24.7$	5.5	21
Pd/0.5 M H ₂ SO ₄ (H ₂ O)	H	$22.8 < \Delta G_{\theta}^{\circ} < 31.8$	14.9	19
Au/0.5 M H ₂ SO ₄ (H ₂ O)	H	$28.7 < \Delta G_{\theta}^{\circ} < 35.6$	11.4	13

Re/0.1 M KOH (H ₂ O)	H	$29.2 < \Delta G_{\theta}^{\circ} < 36.0$	11.4	16
Re/0.5 M H ₂ SO ₄ (H ₂ O)	H	$32.7 < \Delta G_{\theta}^{\circ} < 39.7$	11.4	16
Ni ^c /0.05 M KOH (H ₂ O)	H	$6.6 < \Delta G_{\theta}^{\circ} < 28.3$	36.2	11
Ni ^d /0.1 M LiOH (H ₂ O)	H	$19.9 < \Delta G_{\theta}^{\circ} < 37.8$	29.8	29
Ni ^d /0.5 M H ₂ SO ₄ (H ₂ O)	H	$47.0 < \Delta G_{\theta}^{\circ} < 61.7$	24.6	29
Ti/0.5 M H ₂ SO ₄ (H ₂ O)	H	$63.1 < \Delta G_{\theta}^{\circ} < 79.6$	27.8	23
Zr/0.2 M H ₂ SO ₄ (H ₂ O)	H	$94.4 < \Delta G_{\theta}^{\circ} < 106.5$	20.1	24

Table 5. ^a Pt–Ir (90:10 mass ratio) alloy. ^b Pt–Ir (70:30 mass ratio) alloy. ^c Ni (purity 99.994%) foil. ^d Ni (purity 99.999%) wire. Comparison of the standard Gibbs energies ($\Delta G_{\theta}^{\circ}$) of adsorptions and rates of change (r) of $\Delta G_{\theta}^{\circ}$ with θ ($0.2 < \theta < 0.8$) for the Temkin adsorption isotherms at the noble and highly corrosion-resistant metal and alloy/H₂O and D₂O solution interfaces

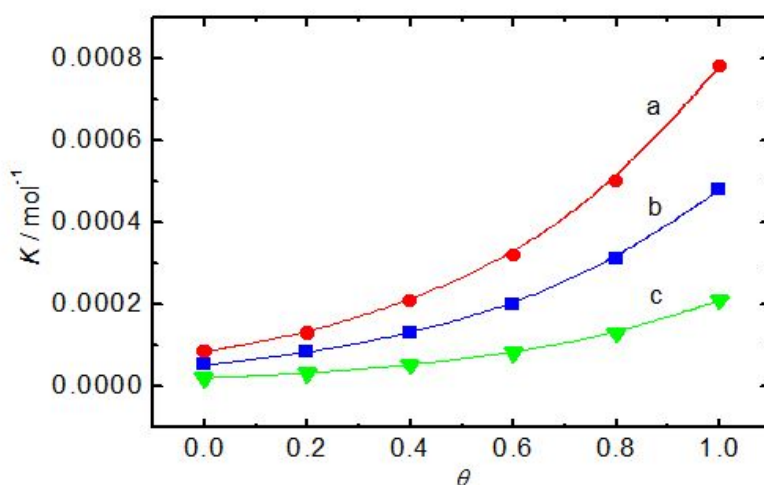


Figure 10. Comparison of the experimentally determined equilibrium constants (K vs. θ) for the Frumkin adsorption isotherms of H, (H + D), and D at the Pt–Ir alloy/0.1 M LiOH solution interfaces. Experimental data calculated using Eq. (6), i.e. the equilibrium constant: (a) 0.1 M LiOH (H₂O) solution (●), (b) 0.1 M LiOH (H₂O + D₂O) solution (■), and (c) 0.1 M LiOH (D₂O) solution (▼).

4.2. Correlation constants between the adsorption isotherms

Curves a, b, c, and d in Fig. 8 show the four numerically calculated Langmuir adsorption isotherms of (H + D) corresponding to $K = 5.3 \times 10^{-3}$, 5.3×10^{-4} , 5.3×10^{-5} , and 5.3×10^{-6} mol⁻¹, respectively. For $0.2 < \theta < 0.8$, all of the Langmuir adsorption isotherms are always parallel to each other [13,16,42]. Correspondingly, all of the slopes of the Langmuir adsorption isotherms, i.e. all of g for the Temkin adsorption isotherms, are all the same regardless of the values of K . As summarized in Tables 2 and 3, we have experimentally and consistently found and confirmed that the values of g for the Temkin adsorption isotherms are approximately 4.6 greater than those for the Langmuir adsorption isotherms, i.e. $g = 0$. Similarly, the values of g for the Temkin adsorption isotherms are approximately 4.6 greater than those for

the Frumkin adsorption isotherms. Because the Frumkin adsorption isotherm is determined on the basis of the Langmuir adsorption isotherm, i.e. $g = 0$ (see Fig. 5).

In addition, we have experimentally and consistently found and confirmed that the equilibrium constants (K_0) for the Temkin adsorption isotherms are approximately 10 times greater than those (K_0 or K) for the correlated Frumkin or Langmuir adsorption isotherms (see Fig. 6 and Tables 2 and 3). These factors (ca. 4.6 and 10) can be taken as correlation constants between the Temkin and Frumkin or Langmuir adsorption isotherms. The two different adsorption isotherms, i.e. the Temkin and Frumkin or Langmuir adsorption isotherms, appear to fit the same data regardless of their adsorption conditions. These aspects are described elsewhere [19, 20, 23–29].

In this work, one can also confirm that the values of g and K_0 for the Temkin adsorption isotherm are approximately 4.6 and 10 times greater than those for the correlated Frumkin adsorption isotherm, respectively. The Temkin adsorption isotherm correlating with the Frumkin adsorption isotherm, and vice versa, is readily determined using the correlation constants. Note that this is a unique feature between the Temkin and Frumkin or Langmuir adsorption isotherms.

4.3. Negative and positive values of the interaction parameters for the Frumkin adsorption isotherms

A negative value of g for the Frumkin adsorption isotherm is qualitatively and quantitatively interpreted elsewhere [42,46]. Negative and positive values of g correspond to lateral attractive and repulsive interactions between the adsorbed species, respectively. At Pt, Ir, and Pt–Ir alloy/H₂O and D₂O solution interfaces, the lateral attractive interaction ($g < 0$) between the adsorbed H, D, or (H + D) species is determined [22]. As stated above, this implies an increase in $|\Delta G_0^\circ|$ of H, D, or (H + D) adsorption with θ ($0 \leq \theta \leq 1$). At Pd, Ni, Ti, and Zr/H₂O solution interfaces, the lateral repulsive interaction ($g > 0$) between the adsorbed H species is determined. This implies a decrease in $|\Delta G_0^\circ|$ of H adsorption with θ ($0 \leq \theta \leq 1$). At Au and Re/H₂O solution interfaces, the lateral interaction between the adsorbed H species is negligible, i.e. $g = 0$ or $g \approx 0$. This implies that the Langmuir adsorption isotherm is applicable. At Pt–Ir alloy/H₂O and D₂O solution interfaces, the lateral repulsive interaction ($g > 0$) between the adsorbed OH or (OH + OD) species is determined. This is significantly different from the lateral attractive interaction ($g < 0$) between the adsorbed H, D, or (H + D) species at the Pt–Ir alloy/H₂O and D₂O solution interfaces.

In contrast to Table 2, Table 3 shows that only the lateral repulsive interaction ($g > 0$) between the adsorbed H, D, (H + D), OH, or (OH + OD) species is determined. This is attributed to the values of g for the Frumkin adsorption isotherms, i.e. $g > -4.6$. Finally, one can conclude that the lateral attractive interaction ($g < 0$) between the adsorbed H, D, or (H + D) species is a unique feature of the Pt, Ir, and Pt–Ir alloy/H₂O and D₂O solution interfaces. The duality of the lateral attractive and repulsive interactions between the adsorbed H, D, or (H + D) species at the Pt, Ir, and Pt–Ir alloy interfaces is attributed to the negative values of g for the Frumkin adsorption isotherms. The Frumkin adsorption isotherm is more useful, effective, and reliable than the Temkin adsorption isotherm. As previously stated, the values of g

for the Frumkin adsorption isotherms have never been experimentally and consistently determined using other conventional methods.

4.4. Equilibrium constants

In the acidic H₂O solutions, the values of K_0 , i.e. K at $g = 0$, for H at the noble metal and alloy (Pt, Ir, Pt–Ir alloy, Pd, Au, Re) interfaces are much greater than those at the highly corrosion-resistant metal (Ni, Ti, Zr) interfaces. In general, the values of K_0 for H in the alkaline H₂O solutions are greater than those in the acidic H₂O solutions. The values of K_0 for H in the acidic H₂O solutions are much greater than those for OH in the alkaline H₂O solutions. In the alkaline H₂O solutions, the values of K_0 for H at the Ni interfaces are greater than those at the Pt, Ir, Pt–Ir alloy, Pd, Au, Re, Ti, and Zr interfaces. This is a unique feature of Ni and Ni alloy/alkaline H₂O solution interfaces. Note that Ni and Ni alloys are the metals most widely used for the cathodic HER in alkaline H₂O solutions.

The lateral interaction between the adsorbed H, D, (H + D), OH, or (OH + OD) species cannot be interpreted by the value of K_0 for the Frumkin adsorption isotherm. For example, the lateral attractive interaction ($g < 0$) between the adsorbed H, D, or (H + D) species at the Pt, Ir, and Pt–Ir alloy interfaces is significantly different from the lateral repulsive interaction ($g > 0$) between the adsorbed H species at the Pd interface even though all of the Pt, Ir, Pt–Ir alloys, and Pd are the same platinum group metals and the values of K_0 for H, D, and (H + D) are similar.

5. Conclusions

The Frumkin and Temkin adsorption isotherms (θ vs. E) of (H + D) and the related electrode kinetic and thermodynamic parameters (g , K , ΔG_0° , r) of the Pt–Ir alloy/0.1 M LiOH (H₂O + D₂O) solution interface have been determined using the phase-shift method and correlation constants and are compared with the relevant experimental data. The value of K decreases with increasing D₂O. The value of K for (H + D) is approximately equal to the average value of K for H and D isotopes. The Frumkin adsorption isotherms of H, D, and (H + D) are readily distinguishable at the interface. For $0.2 < \theta < 0.8$, the lateral attractive ($g < 0$) or repulsive ($g > 0$) interaction between the adsorbed (H + D) species appears at the interface. The Temkin adsorption isotherm correlating with the Frumkin or Langmuir adsorption isotherm, and vice versa, is readily determined using the correlation constants.

The lateral attractive interaction ($g < 0$) between the adsorbed H, D, or (H + D) species appears at the Pt, Ir, and Pt–Ir alloy interfaces. The lateral repulsive interaction ($g > 0$) between the adsorbed H species appears at the Pd, Ni, Ti, and Zr interfaces. At the Au and Re interfaces, the lateral interaction between the adsorbed H species is negligible, i.e. $g = 0$ or $g \approx 0$. The lateral repulsive interaction ($g > 0$) between the adsorbed OH or (OH + OD) species appears at the Pt–Ir alloy interfaces. The lateral attractive interaction ($g < 0$) between the adsorbed H, D, or (H + D) species is a unique feature of the Pt, Ir, and Pt–Ir alloy interfaces. For $0.2 < \theta < 0.8$, the duality of the lateral attractive and repulsive interactions between the ad-

sorbed H, D, or (H + D) species appears at the Pt, Ir, and Pt–Ir alloy interfaces. This unique feature of the Pt, Ir, and Pt–Ir alloy interfaces is attributed to the range of g for the Frumkin adsorption isotherms of H, D, and (H + D), i.e. $-4.6 < g < 0$.

The phase-shift method and correlation constants are the most accurate and efficient techniques to determine the Frumkin, Langmuir, and Temkin adsorption isotherms and the related electrode kinetic and thermodynamic parameters of the noble and highly corrosion-resistant metal and alloy/H₂O and D₂O solution interfaces. They are useful and effective in facilitating selection of optimal electrode materials to yield electrochemical systems of maximum hydrogen, deuterium, and oxygen evolution performances. We expect that numerical simulations with a single equation for $-\varphi$ vs. θ as functions of E and f or relevant experimental data for the phase-shift method and correlation constants will be obtained, compared, and discussed by other investigators.

Acknowledgements

The authors would like to thank Dr. Mu S. Cho (First President of Kwangwoon University, Seoul, Republic of Korea) for supporting the EG&G PAR 273A potentiostat/galvanostat, Schlumberger SI 1255 HF frequency response analyzer, and software packages. The section on theoretical and experimental backgrounds of the phase-shift method was reprinted with permission from Journal of Chemical & Engineering Data 55 (2010) 5598–5607. Copyright 2010 American Chemical Society. The authors wish to thank the American Chemical Society. This work was supported by the Research Grant of Kwangwoon University in 2012.

Author details

Jinyoung Chun¹ and Jang H. Chun^{2*}

*Address all correspondence to: jhchun@kw.ac.kr

1 Department of Chemical Engineering, Pohang University of Science and Technology, Pohang, Kyungbuk, Republic of Korea

2 Department of Electronic Engineering, Kwangwoon University, Seoul, Republic of Korea

References

- [1] Gileadi, E., Kirowa-Eisner, E., & Penciner, J. (1975). Interfacial electrochemistry. Reading MA: Addison-Wesley.
- [2] Gileadi, E. (1993). Electrode kinetics. New York: VCH.

- [3] Conway, B. E., & Jerkiewicz, G. (1995). Electrochemistry and materials science of cathodic hydrogen absorption and adsorption. *Electrochemical Society Proceedings*, 94, Pennington, NJ: The Electrochemical Society.
- [4] Jerkiewicz, G., & Marcus, P. (1997). Electrochemical surface science and hydrogen adsorption and absorption. *Electrochemical Society Proceedings*, 97, Pennington, NJ: The Electrochemical Society.
- [5] Jerkiewicz, G. (1998). Hydrogen sorption at/in electrodes. *Prog. Surf. Sci.*, 57(2), 137-186.
- [6] Jerkiewicz, G., Feliu, J. M., & Popov, B. N. (2000). Hydrogen at surface and interfaces. *Electrochemical Society Proceedings*, 2000-16, Pennington, NJ: The Electrochemical Society.
- [7] Jerkiewicz, G. (2010). Electrochemical hydrogen adsorption and absorption. Part 1: Under-potential deposition of hydrogen. *Electrocatal*, 1(4), 179-199.
- [8] Gileadi, E. (1967). Adsorption in electrochemistry. *Gileadi E, editor. Electrosorption*. New York: Plenum Press, 1.
- [9] Chun, J. H., & Ra, K. H. (1998). The phase-shift method for the Frumkin adsorption isotherms at the Pd/H₂SO₄ and KOH solution interfaces. *J. Electrochem. Soc.*, 145(11), 3794-3798.
- [10] Chun, J. H., Ra, K. H., & Kim, N. Y. (2001). The Langmuir adsorption isotherms of electroadsorbed hydrogens for the cathodic hydrogen evolution reactions at the Pt(100)/H₂SO₄ and LiOH aqueous electrolyte interfaces. *Int. J. Hydrogen Energy*, 26(9), 941-948.
- [11] Chun, J. H., Ra, K. H., & Kim, N. Y. (2002). Qualitative analysis of the Frumkin adsorption isotherm of the over-potentially deposited hydrogen at the poly-Ni/KOH aqueous electrolyte interface using the phase-shift method. *J. Electrochem. Soc.*, 149(9), E325-330.
- [12] Chun, J. H., & Jeon, S. K. (2003). Determination of the equilibrium constant and standard free energy of the over-potentially deposited hydrogen for the cathodic H₂ evolution reaction at the Pt-Rh alloy electrode interface using the phase-shift method. *Int. J. Hydrogen Energy*, 28(12), 1333-1343.
- [13] Chun, J. H., Ra, K. H., & Kim, N. Y. (2003). Langmuir adsorption isotherms of over-potentially deposited hydrogen at poly-Au and Rh/H₂SO₄ aqueous electrolyte interfaces: Qualitative analysis using the phase-shift method. *J. Electrochem. Soc.*, 150(4), E207-217.
- [14] Chun, J. H. (2003). Methods for estimating adsorption isotherms in electrochemical systems. *U.S. Patent*, 6613218.
- [15] Chun, J. H., Jeon, S. K., Kim, B. K., & Chun, J. Y. (2005). Determination of the Langmuir adsorption isotherms of under- and over-potentially deposited hydrogen for

the cathodic H₂ evolution reaction at poly-Ir/aqueous electrolyte interfaces using the phase-shift method. *Int. J. Hydrogen Energy*, 30(3), 247-259.

- [16] Chun, J. H., Jeon, S. K., Ra, K. H., & Chun, J. Y. (2005). The phase-shift method for determining Langmuir adsorption isotherms of over-potentially deposited hydrogen for the cathodic H₂ evolution reaction at poly-Re/aqueous electrolyte interfaces. *Int. J. Hydrogen Energy*, 30(5), 485-499.
- [17] Chun, J. H., Jeon, S. K., Kim, N. Y., & Chun, J. Y. (2005). The phase-shift method for determining Langmuir and Temkin adsorption isotherms of over-potentially deposited hydrogen for the cathodic H₂ evolution reaction at the poly-Pt/H₂SO₄ aqueous electrolyte interface. *Int. J. Hydrogen Energy*, 30(13-14), 1423-1436.
- [18] Chun, J. H., & Kim, N. Y. (2006). The phase-shift method for determining adsorption isotherms of hydrogen in electrochemical systems. *Int. J. Hydrogen Energy*, 31(2), 277-283.
- [19] Chun, J. H., Jeon, S. K., & Chun, J. Y. (2007). The phase-shift method and correlation constants for determining adsorption isotherms of hydrogen at a palladium electrode interface. *Int. J. Hydrogen Energy*, 32(12), 1982-1990.
- [20] Chun, J. H., Kim, N. Y., & Chun, J. Y. (2008). Determination of adsorption isotherms of hydrogen and hydroxide at Pt-Ir alloy electrode interfaces using the phase-shift method and correlation constants. *Int. J. Hydrogen Energy*, 33(2), 762-774.
- [21] Chun, J. H., & Chun, J. Y. (2008). Correction and supplement to the determination of the optimum intermediate frequency for the phase-shift method [Chun et al., *Int. J. Hydrogen Energy* 30 (2005) 247-259, 1423-1436]. *Int. J. Hydrogen Energy*, 33(19), 4962-4965.
- [22] Chun, J. Y., & Chun, J. H. (2009). A negative value of the interaction parameter for over-potentially deposited hydrogen at Pt, Ir, and Pt-Ir alloy electrode interfaces. *Electrochem. Commun*, 11(4), 744-747.
- [23] Chun, J. Y., & Chun, J. H. (2009). Determination of adsorption isotherms of hydrogen on titanium in sulfuric acid solution using the phase-shift method and correlation constants. *J. Chem. Eng. Data*, 54(4), 1236-1243.
- [24] Chun, J. H., & Chun, J. Y. (2009). Determination of adsorption isotherms of hydrogen on zirconium in sulfuric acid solution using the phase-shift method and correlation constants. *J. Korean Electrochem. Soc*, 12(1), 26-33.
- [25] Chun, J., Lee, J., & Chun, J. H. (2010). Determination of adsorption isotherms of over-potentially deposited hydrogen on platinum and iridium in KOH aqueous solution using the phase-shift method and correlation constants. *J. Chem. Eng. Data*, 55(7), 2363-2372.
- [26] Chun, J., Kim, N. Y., & Chun, J. H. (2010). Determination of adsorption isotherms of hydroxide and deuterioxide on Pt-Ir alloy in LiOH solutions using the phase-shift method and correlation constants. *J. Chem. Eng. Data*, 55(9), 3825-3833.

- [27] Chun, J., Kim, N. Y., & Chun, J. H. (2010). Determination of the adsorption isotherms of hydrogen and deuterium isotopes on a Pt-Ir alloy in LiOH solutions using the phase-shift method and correlation constants. *J. Chem. Eng. Data*, 55(12), 5598-5607.
- [28] Chun, J., Kim, N. Y., & Chun, J. H. (2011). Determination of the adsorption isotherms of overpotentially deposited hydrogen on a Pt-Ir alloy in H₂SO₄ aqueous solution using the phase-shift method and correlation constants. *J. Chem. Eng. Data*, 56(2), 251-258.
- [29] Chun, J. H. (2012). Determination of the Frumkin and Temkin adsorption isotherms of hydrogen at nickel/acidic and alkaline aqueous solution interfaces using the phase-shift method and correlation constants. *J. Korean Electrochem. Soc*, 15(1), 54-66.
- [30] Kvastek, K., & Horvat-Radosevic, V. (2004). Comment on: Langmuir adsorption isotherms of over-potentially deposited hydrogen at poly-Au and Rh/H₂SO₄ aqueous electrolyte interfaces; Qualitative analysis using the phase-shift method. *J. Electrochem. Soc*, 151(9), L9-10.
- [31] Chun, J. H., Ra, K. H., & Kim, N. Y. (2004). Response to comment on: Langmuir adsorption isotherms of over-potentially deposited hydrogen at poly-Au and Rh/H₂SO₄ aqueous electrolyte interfaces; Qualitative analysis using the phase-shift method. *J. Electrochem. Soc* 150 (2003) E207-217. *J. Electrochem. Soc*, 151(9), L11-13.
- [32] Lasia, A. (2005). Comments on: The phase-shift method for determining Langmuir adsorption isotherms of over-potentially deposited hydrogen for the cathodic H₂ evolution reaction at poly-Re/aqueous electrolyte interfaces. *Int. J. Hydrogen Energy* 30 (2005) 485-499. *Int. J. Hydrogen Energy*, 30(8), 913-917.
- [33] Chun, J. H., Jeon, S. K., Kim, N. Y., & Chun, J. Y. (2005). Response to comments on: The phase-shift method for determining Langmuir adsorption isotherms of over-potentially deposited hydrogen for the cathodic H₂ evolution reaction at poly-Re/aqueous electrolyte interfaces. *Int. J. Hydrogen Energy* 30 (2005) 485-499. *Int. J. Hydrogen Energy*, 30(8), 919-928.
- [34] Horvat-Radosevic, V., & Kvastek, K. (2009). Pitfalls of the phase-shift method for determining adsorption isotherms. *Electrochem. Commun*, 11(7), 1460-1463.
- [35] In our e-mail communications, Horvat-Radosevic et al. admitted that all of their objections to the phase-shift method in Ref. 34 were confused and misunderstood. The exact same confusion and misunderstanding about the phase-shift method also appear in Refs. 30 and 32.
- [36] Gileadi, E., Kirowa-Eisner, E., & Penciner, J. (1975). *Interfacial electrochemistry*. Reading, MA: Addison-Wesley, 6.
- [37] Gileadi, E., Kirowa-Eisner, E., & Penciner, J. (1975). *Interfacial electrochemistry*. Reading, MA: Addison-Wesley, 86.

- [38] Harrington, D. A., & Conway, B. E. (1987). AC impedance of faradaic reactions involving electrosorbed intermediates-I. Kinetic theory. *Electrochim. Acta*, 32(12), 1703-1712.
- [39] Gileadi, E. (1993). Electrode kinetics. *New York: VCH*, 291.
- [40] Gileadi, E. (1993). Electrode kinetics. *New York: VCH*, 307.
- [41] Gileadi, E., Kirowa-Eisner, E., & Penciner, J. (1975). Interfacial electrochemistry. *Reading, MA: Addison-Wesley*, 82.
- [42] Gileadi, E. (1993). Electrode kinetics. *New York: VCH*, 261.
- [43] Bockris, J., O'M Reddy, A. K. N., & Gamboa-Aldeco, M. (2000). Modern electrochemistry. 2nd edition. *New York: Kluwer Academic/Plenum Press*, 2A, 1193.
- [44] Oxtoby, D. W., Gillis, H. P., & Nachtrieb, N. H. (2002). Principles of modern chemistry. 5th edition. *New York: Thomson Learning Inc*, 446.
- [45] Bockris, J., & O'M Khan, S. U. M. (1993). Surface electrochemistry. *New York: Plenum Press*, 596.
- [46] Gileadi, E. (1993). Electrode kinetics. *New York: VCH*, 303.

IntechOpen

